nature geoscience

LETTERS

PUBLISHED ONLINE: 9 JUNE 2013 | DOI: 10.1038/NGEO1837

Intensification of open-ocean oxygen depletion by vertically migrating animals

Daniele Bianchi[1]*, Eric D. Galbraith[1], David A. Carozza[1], K. A. S. Mislan[2] and Charles A. Stock[3]

Throughout the ocean, countless small animals swim to depth in the daytime, presumably to seek refuge from large predators[1,2]. These animals return to the surface at night to feed[1,2]. This substantial diel vertical migration can result in the transfer of significant amounts of carbon and nutrients from the surface to depth[3–7]. However, its consequences on ocean chemistry at the global scale have remained uncertain[8,9]. Here, we determine the depths of these diel migrations in the global ocean using a global array of backscatter data from acoustic Doppler current profilers, collected between 1990 and 2011. We show that the depth of diel migration follows coherent large-scale patterns. We find that migration depth is greater where subsurface oxygen concentrations are high, such that seawater oxygen concentration is the best single predictor of migration depth at the global scale. In oxygen minimum zone areas, migratory animals generally descend as far as the upper margins of the low-oxygen waters. Using an ocean biogeochemical model coupled to a general circulation model, we show that by focusing oxygen consumption in poorly ventilated regions of the upper ocean, diel vertical migration intensifies oxygen depletion in the upper margin of oxygen minimum zones. We suggest that future changes in the extent of oxygen minimum zones could alter the migratory depths of marine organisms, with consequences for marine biogeochemistry, food webs and fisheries.

The concentrations of dissolved oxygen in the ocean are determined by the interplay of the three-dimensional circulation and a wide range of ecosystem processes. The complexity of the marine ecosystem is overwhelmingly evident from the vast diversity of oceanic life, but this complexity must be greatly idealized in any attempt to quantify its role in ocean biogeochemistry. Among the typical simplifications of ocean biogeochemistry models, the respiration of organic matter in the subsurface is generally treated as the work of ubiquitous microbes feeding on organic particles that settle passively through the water column, ignoring the potential role of animals in the transport and respiration of organic matter. However, the biomass of animals is large (>2.5 Pg; ref. 10), comparable to that of phytoplankton, and their motility makes their effect potentially very different from that of passive microbes. Although animals exhibit a daunting array of behaviours in the marine environment, many of which remain poorly understood, a common observed behaviour is the diel vertical migration (DVM).

The pervasive occurrence of DVM has long been recognized by the oceanographic community. Increased night-time catches near the surface became evident in oceanographic surveys of the early twentieth century and provided the first documented evidence of DVM (ref. 11). Extensive acoustic surveys subsequently revealed sound scattering layers that migrated on a diurnal basis between the surface and mid-depths[1,12], and it became clear that mesopelagic fish of the myctophid family were responsible for much of the sound scattering, because of their abundance and the acoustic properties of their gas bladders[13]. However, the dominance of myctophids in producing the acoustic signal does not mean that they travel alone; detailed *in situ* sampling has shown very close association of a variety of taxa within or around the depths of the scattering layers, including siphonophores, cephalopods, copepods, euphausiids and salps[1,2,5,13–16]. Presumably, many migrators benefit from reduced visual predation in the dark mesopelagic ocean, compensating for the energetic costs of migrations over distances that can exceed their body length by 5 orders of magnitude[17].

Despite the long history of DVM studies, there have been few efforts to quantify the role of DVM in global-scale biogeochemical cycling[3,9]. Studies at individual sites suggest that the active transport of organic matter by mesozooplankton and micronekton that feed at the surface but metabolize and excrete at depth, ranges typically between around 10–50% of the local sinking flux of organic particles[3–7] (see also Supplementary Table S1). However, evaluating the global biogeochemical impact of DVM requires taking ocean circulation into account; oxygen losses from respiring migrators in well-ventilated waters will be quickly erased, whereas oxygen losses in stagnant corners of the ocean will accumulate. The depth to which migrators swim would be expected to play a key role in determining the biogeochemical impact of migration because the rate of ocean ventilation decreases rapidly with depth—but there have been no previous attempts to predict daytime migration depths at the global scale.

To develop a global view of daytime DVM depths, we analysed acoustic Doppler current profiler (ADCP) measurements from 389 cruises conducted between 1990 and 2011 (Methods). These acoustic data typically show periodic migrations from the surface to depths of 200–650 m before sunrise, little change through the daytime, and reverse migrations before sunset (Fig. 1). Despite including data from different seasons over a time span of two decades, the distribution of daytime DVM depths derived from the acoustic data (Fig. 2) reveals remarkably coherent patterns. Daytime DVM depths of up to 650 m are observed in the central regions of the subtropical gyres, whereas daytime DVM depths as shallow as 200 m are found in the North Pacific subpolar gyre, the Eastern Tropical Pacific, the Northern Indian Ocean and the high-latitude North Atlantic, consistent with local acoustic surveys and *in situ* biomass measurements[5,13,15,16,18].

The coherency of these regional patterns suggests that the oceanic environment exerts a strong control on DVMs, either by directly modulating their daytime depths, or by changing the composition of migratory populations, which in turn affects migration depths. It has long been argued that light regulates DVM (ref. 11) either by setting a preferred isolume that guides organisms during migrations or triggering migrations through changes

[1]Department of Earth and Planetary Sciences, McGill University, 3450, Rue University, Montreal, Quebec H3A 2A7, Canada, [2]Department of Atmospheric and Ocean Sciences, Princeton University, 300 Forrestal Road, Sayre Hall, Princeton, New Jersey 08544, USA, [3]NOAA Geophysical Fluid Dynamics Laboratory, 201 Forrestal Road, Princeton, New Jersey 08540, USA. *e-mail: daniele.bianchi@mail.mcgill.ca

© 2013 Macmillan Publishers Limited. All rights reserved.

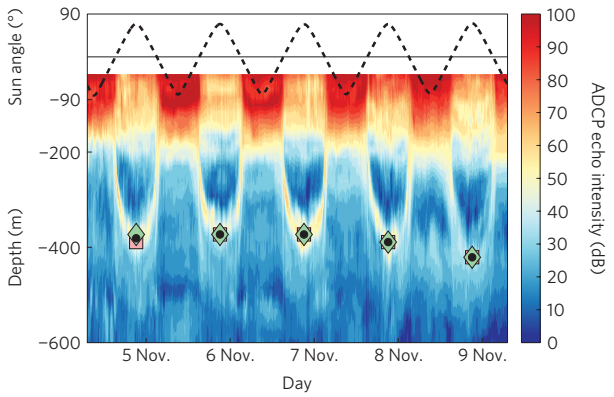

Figure 1 | Vertical migration as observed with acoustic data. Time series of ADCP echo intensities (colour contours, decibel) and daytime DVM depths (symbols) for the Japanese cruise KY0312 in the western equatorial Pacific Ocean (five days, between 5 and 9 November 2003; 146.2° W, 8.8° N to 147.0° W, 2. 5° N). The echo intensity has been corrected by subtracting the lowest 10% of data. The black dashed line shows the local Sun elevation angle (°). The pink squares, green diamonds and black dots indicate respectively: the daytime DVM depth estimated from day-to-night maximum echo intensity change, the daytime DVM depth estimated from the daytime maximum subsurface backscatter, and the average of the two (see Methods). Note that −90 on the *x* axis refers to both Sun angle (°) and depth (m).

in irradiance, or through combinations of both mechanisms[19]. However, when we compare the observed pattern of daytime DVM depths to calculated subsurface light intensities, we find only a weak relationship at the global scale (Supplementary Information and Figs S4 and S5). Instead, we find the strongest correlation between daytime DVM depths and oxygen concentrations, whether by comparison with the average oxygen concentration in the upper mesopelagic zone (150–500 m, $R^2 = 0.37$, $p < 0.01$) or with the oxygen gradient between the surface (0–25 m) and the upper mesopelagic zone ($R^2 = 0.45$, $p < 0.01$). Where the major oxygen minimum zones occur, migrators penetrate into the oxygen minima, where they remain during daytime, in many cases reaching their cores (Supplementary Fig. S7), in agreement with previous local studies[13,15,16]. This observation is consistent with the hypothesis that low oxygen concentrations provide a refuge from large visual predators[5,20], which are generally vigorous swimmers with larger body sizes and higher oxygen requirements than their prey[20,21]. It would follow from this hypothesis that in many regions where no oxygen minimum zone occurs, vertical migrators must head to greater depths to find refuge from predators. Regular nighttime migrations back to the surface would not only allow feeding while minimizing predatory pressure, but would also replenish any oxygen debt developed during the diurnal stay in deeper, oxygen-depleted waters[20].

Although oxygen distribution explains the largest single fraction of the variance in the observed daytime DVM depths, a stepwise linear regression that also includes surface chlorophyll, mixed-layer depths and temperature gradients provides an even better prediction ($R^2 = 0.60$, $p < 0.01$, Methods). The statistical relationship between the depth of DVM and environmental variables provides a means by which to assess the global biogeochemical role of DVM. To simultaneously account for the effects of respiration of migrators and ocean circulation, we use a prognostic ocean ecosystem model coupled to a general circulation model[22]. In the model, organic matter, produced by photosynthesis as a function of light, temperature and nutrients, is partitioned between dissolved and particulate organic matter. In the control simulation, the sinking particle flux is respired according to a simple power-law profile[23]. To elucidate the primary biogeochemical changes due to vertical migrations, we apportion a fraction of the particulate organic matter production to active transport by migrators (Methods). We then distribute the migratory respiration between the surface and the vicinity of the daytime DVM depth, in proportion to an estimate of the time spent at each depth (Methods). Given the uncertainty in the fraction of export production due to migrating animals, we varied the global active-export fraction across the range of values suggested by observations[3–7] (see also Supplementary Table S1). Although it is likely that the active DVM export fraction varies regionally, the constant value here provides a useful first estimate. The results show an approximately linear relationship between the active export fraction and the amount of oxygen consumed by migrators (Methods), which allows us to present the consumption of oxygen as a function of the active export fraction, shown in Fig. 3.

Effectively, active DVM transport extracts a small fraction of organic matter from the well-ventilated and productive surface ocean, and focuses its respiration at generally poorly ventilated depths (Fig. 3). Thus, the impact of the active export fraction is strongly amplified at the migration depth, to represent a surprisingly large fraction of the oxygen consumption near that depth. For example, DVM export fractions of 10–30% predict

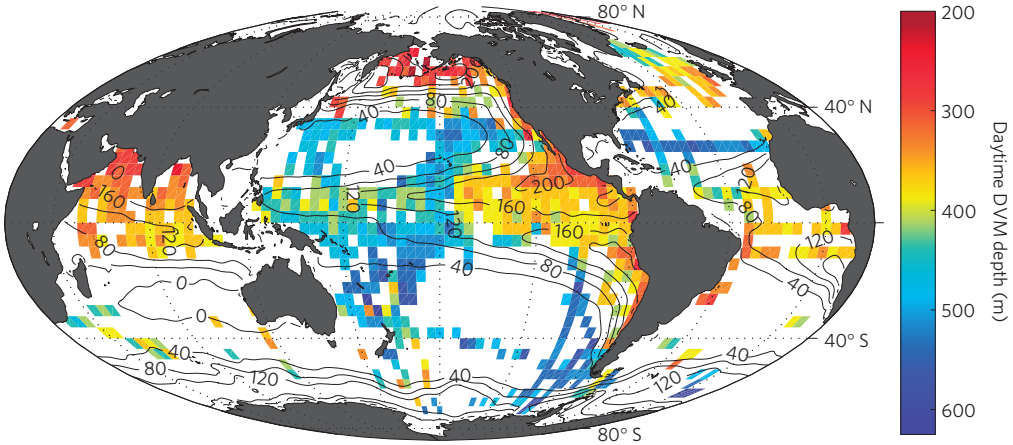

Figure 2 | Observed daytime DVM depths (m) and surface to mesopelagic oxygen gradients (mmol m^{-3}). Map of daytime DVM depths (colours) from acoustic data averaged on 4° × 4° areas, and surface (0–25 m) to upper mesopelagic zone (150–500 m) oxygen difference (contours). Shallowest migrations are shown in red, deepest migrations in blue. Large surface to mid-depth oxygen gradients are observed on top of the major open ocean oxygen minimum zones. Linear correlation with surface to mid-depth oxygen gradients alone explains 45% of the DVM depth variance (see Methods).

© 2013 Macmillan Publishers Limited. All rights reserved.

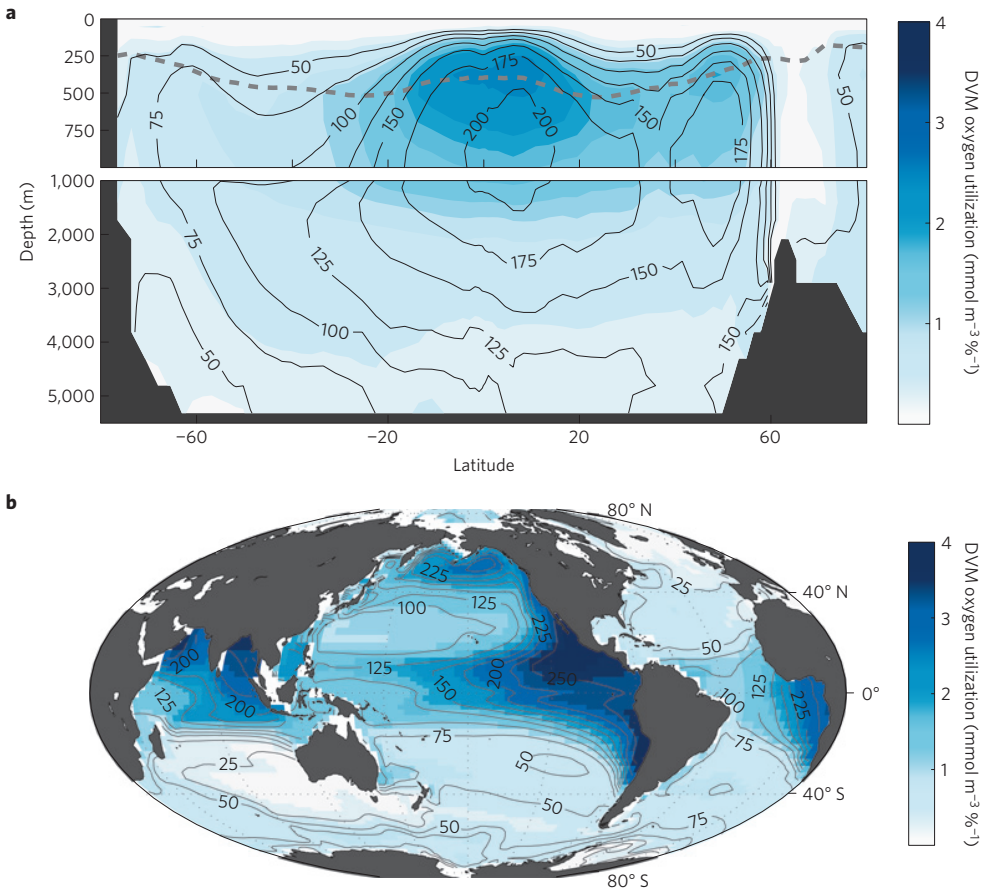

Figure 3 | Simulated impact of DVM respiration on dissolved oxygen. Colour shadings show the modelled oxygen utilization due to DVM for every 1% of export by DVM relative to particle export, expressed in mmol m^{-3} $\%^{-1}$. For example, given a global DVM export fraction of 10%, the deepest blue indicates an oxygen utilization of 40 mmol m^{-3}. Solid contours show the modelled total oxygen utilization (mmol m^{-3}). **a**, Zonal average. The grey dashed line indicates the mean daytime DVM depth in the model. **b**, Average over the upper mesopelagic zone (150–500 m).

oxygen utilizations by migrating organisms of 15–46 mmol m^{-3}, averaged globally over the upper mesopelagic zone (150–500 m). This is equivalent to 17–75% of the oxygen utilization due to passive export in that depth range. The DVM oxygen depletion is particularly significant in the upper layers of the oxygen minimum zones of the ocean thermocline (Fig. 3). These oxygen-depleted waters host hypoxic and suboxic cores[24] that aerobic migrators must either avoid, or enter while temporarily relying on metabolic adaptations to low oxygen levels[20,25]. In either case, the aerobic demand of the migrators would be focused on the hypoxic and suboxic upper margins of the oxygen minimum zone, exerting an important control on oxygen depletion there.

The strong influence of DVM on oxygen minimum zones is particularly intriguing given the observed correlation between oxygen minimum zones and vertical migrations. The oxygen drawdown induced by DVM, although significant, is not enough to produce the oxygen minimum zones *ab initio*—the locations of the main oxygen minima are determined by the large-scale ocean circulation[26]. However, the respiration by small, hypoxia-tolerant animals undergoing DVM seems to be important in establishing the geometry and intensity of oxygen minimum zones. The possibility of feedbacks between DVM and oxygen minima, through their potential role as refuges from predators[20,21], deserves further attention.

Our findings show a coupling between migrating marine animals and oxygen distribution in the ocean. Furthermore, they indicate that the role of DVM in subsurface oxygen consumption is of first-order importance, particularly in poorly ventilated regions of the upper ocean. Further quantifications of this coupling will require new observational constraints on the partitioning of export between active migrators and passive sinking, the role of animals on particle dynamics, particularly in the mesopelagic ecosystem[8,9], the dependence of animal metabolism on dissolved oxygen[20,25], and the rates of animal respiration within oxygen minima[6]. Such constraints are critical given predictions of widespread ocean deoxygenation in response to anthropogenic climate change[27]. Expansions of oxygen minimum zones could alter the patterns of DVM through changes in migrating organisms' habitat and migratory depths, with implications for marine food webs and fisheries[21]. Conversely, changes in the abundance of vertical migrators[28] that may be attributable to natural fluctuations, climate change or the removal of animal species by fisheries have the potential to affect ocean biogeochemistry in previously unforeseen ways.

Methods

Analysis of daytime DVM depths. We analysed 389 cruises out of 1,455 cruises from the US National Oceanic Data Center Joint Archive for Shipboard ADCP and from the British Oceanographic Data Center. We included cruises in which the temporal and vertical resolution of the ADCP data allowed for the detection of one or more DVM events, and focused on migrations that reached the mesopelagic domain, thus excluding DVM migrations shallower than approximately 150–200 m. The ADCP frequencies in the data set, ranging between 38 and 150 kHz, are able to reveal scattering layers composed by millimetre- to centimeter-scale zooplankton and micronekton[15,16]. Although the composition of the sound scattering layers cannot be univocally determined by ADCP data, several empirical studies have shown good correlations between backscatter intensities and zooplankton and micronekton biomass[15,16,29,30]. For each DVM event (4,640 in total) we estimated the daytime DVM depth from: the maximum subsurface day-to-night echo intensity difference and the maximum subsurface daytime backscatter

© 2013 Macmillan Publishers Limited. All rights reserved.

(Supplementary Information), focusing on the layer that returned the strongest signal in the case of multiple scattering layers. The two methods provided identical depths for 38% of the events, and depths differing by less than 50 m for 80% of the events (Supplementary Fig. S1). Some uncertainty in daytime DVM depth still remains, due to the nature of the data and of the analysis. However, the DVM events that show differences larger than 100 m are only 7% of the total, a relatively minor fraction that does not significantly impact our results. Whenever both methods provided a valid daytime DVM depth, the average was taken. Migration depths were averaged over $4° \times 4°$ areas to generate the map in Fig. 2.

Regression between oceanographic properties and DVM depth. We developed an empirical predictive model for daytime DVM depths (Z_{DVM}, m) based on a stepwise multiple linear regression with environmental variables. We obtained a good fit to the data ($R^2 = 0.60$, $p < 0.01$, Supplementary Fig. S6) by using the following set of predictors: oxygen and temperature gradients (ΔO_2, mmol m^{-3}, and ΔT, °C) between the surface (0–25 m) and the upper mesopelagic zone (150–500 m), $\log_{10}$ of surface chlorophyll (Chl, mg m^{-3}) and mixed-layer depth (mld, m). These variables were sampled at the locations and months of each DVM event, using global monthly climatological data sets (see references in the Supplementary Information). This resulted in the following regression (factors listed in order of importance):

$$Z_{DVM} = 398 - 0.56 \cdot \Delta O_2 - 115 \cdot \mathrm{Log}_{10}(\mathrm{Chl}) + 0.36 \cdot \mathrm{mld} - 2.4 \cdot \Delta T$$

Although more complex models can be devised, the simple linear regression was sufficient to explain a large portion of the DVM patterns. Similar results can be obtained using net primary production instead of chlorophyll. Here, we use chlorophyll because worldwide estimates of net primary production and export production are generally based on empirical relationships that rely on chlorophyll and temperature observations. Physical and biogeochemical properties vary in concert in the ocean and are not completely uncorrelated. However, within the uncertainty bounds, we obtain the same coefficients after linear regularization of the regression. Finally, we note that the use of climatological data can introduce biases due to smoothing and interpolation artefacts, the effects of variability in ocean circulation and biogeochemistry on multiple temporal and spatial scales, and potential systematic errors in early measurements (for example, ref. 24). However, the global-scale nature of the analysis, and the lack of exhaustive *in situ* data synchronous with the ADCP measurements, motivated the use of global climatologies.

Ocean circulation–biogeochemistry model. We use the 3-degree GFDL MOM4p1 ocean model coupled with the BLINGv0 biogeochemistry model[22]. BLING includes macronutrient, micronutrient and light limitation, and an implicit treatment of ecosystem structure. Organic matter produced by photosynthesis is partitioned between a dissolved pool, sinking particle and active DVM fluxes. We assume that the DVM export is a constant fraction of the particle production, and vary this fraction between 0 and 45%, spanning the range of observational estimates (Supplementary Table S1). DVM export is remineralized with a profile centred at the daytime DVM depth, calculated from model variables using the data-based multiple linear regression (Supplementary Information and Figs S8 and S9). Oxygen respiration is tied to phosphate remineralization through a stoichiometric ratio of 150:1, and is set to zero at oxygen concentrations lower than 1.0 mmol m^{-3}. The models were integrated for 1,500 years, and the last 100 years were analysed. In the models, the oxygen utilization due to migrators shows an approximately linear dependency with the active export fraction at any given location (Supplementary Fig. S10). This result allows us to use the different model runs to calculate the slope between the active export fraction and the oxygen utilization due to DVM, and express it in units of millimoles per cubic metre for every 1% of export by DVM relative to particle export, as shown in Fig. 3.

Received 15 November 2012; accepted 30 April 2013; published online 9 June 2013

References

1. Vinogradov, M. E. *Vertical Distribution of the Oceanic Zooplankton* (Nauka, 1968).
2. Longhurst, A. R. *The Ecology of the Seas* 116–137 (Blackwell Science, 1976).
3. Longhurst, A. R. & Harrison, W. G. Vertical nitrogen flux from the oceanic photic zone by diel migrant zooplankton and nekton. *Deep-Sea Res. I* **35,** 881–889 (1988).
4. Zhang, X. S. & Dam, H. G. Downward export of carbon by diel migrant mesozooplankton in the central equatorial Pacific. *Deep-Sea Res. II* **44,** 2191–2202 (1997).
5. Steinberg, D. K., Cope, J. S., Wilson, S. E. & Kobari, T. A comparison of mesopelagic mesozooplankton community structure in the subtropical and subarctic North Pacific Ocean. *Deep-Sea Res. II* **55,** 1615–1635 (2008).
6. Hernandez-Leon, S. & Ikeda, T. *Respiration in Aquatic Environment* 57–82 (Oxford Univ. Press, 2005).
7. Hidaka, K., Kawaguchi, K., Murakami, M. & Takahashi, M. Downward transport of organic carbon by diel migratory micronekton in the western equatorial Pacific: Its quantitative and qualitative importance. *Deep-Sea Res. I* **48,** 1923–1939 (2001).
8. Robinson, C. *et al.* Mesopelagic zone ecology and biogeochemistry—a synthesis. *Deep-Sea Res. II* **57,** 1504–1518 (2010).
9. Buesseler, K. O. & Boyd, P. W. Shedding light on processes that control particle export and flux attenuation in the twilight zone of the open ocean. *Limnol. Oceanogr.* **54,** 1210–1232 (2009).
10. Jennings, S. *et al.* Global-scale predictions of community and ecosystem properties from simple ecological theory. *Proc. R. Soc. B* **275,** 1375–1383 (2008).
11. Murray, J. & Hjort, J. *The Depths of the Ocean* (Macmillan, 1912).
12. Eyring, C. F., Christensen, R. J. & Raitt, R. W. Reverberation in the Sea. *J. Acoust. Soc. Am.* **20,** 462–475 (1948).
13. Barham, E. G. Deep scattering layer migration and composition—observations from a diving saucer. *Science* **151,** 1399 (1966).
14. Roe, H. S. J. *et al.* The diel migrations and distributions within a mesopelagic community in the Northeast Atlantic. 1. Introduction and sampling procedures. *Prog. Oceanogr.* **13,** 245–268 (1984).
15. Luo, J. G., Ortner, P. B., Forcucci, D. & Cummings, S. R. Diel vertical migration of zooplankton and mesopelagic fish in the Arabian Sea. *Deep-Sea Res. II* **47,** 1451–1473 (2000).
16. Ashjian, C. J., Smith, S. L., Flagg, C. N. & Idrisi, N. Distribution, annual cycle, and vertical migration of acoustically derived biomass in the Arabian Sea during 1994–1995. *Deep-Sea Res. II* **49,** 2377–2402 (2002).
17. Lampert, W. The adaptive significance of diel vertical migration of zooplankton. *Funct. Ecol.* **3,** 21–27 (1989).
18. Wishner, K. F., Gowing, M. M. & Gelfman, C. Mesozooplankton biomass in the upper 1000 m in the Arabian Sea: Overall seasonal and geographic patterns, and relationship to oxygen gradients. *Deep-Sea Res. II* **45,** 2405–2432 (1998).
19. Cohen, J. H. & Forward, R. B. Zooplankton diel vertical migration—a review of proximate control. *Oceanogr. Mar. Biol.* **47,** 77–109 (2009).
20. Seibel, B. A. Critical oxygen levels and metabolic suppression in oceanic oxygen minimum zones. *J. Exp. Biol.* **214,** 326–336 (2011).
21. Stramma, L. *et al.* Expansion of oxygen minimum zones may reduce available habitat for tropical pelagic fishes. *Nature Clim. Change* **2,** 33–37 (2012).
22. Galbraith, E. D., Gnanadesikan, A., Dunne, J. P. & Hiscock, M. R. Regional impacts of iron-light colimitation in a global biogeochemical model. *Biogeosciences* **7,** 1043–1064 (2010).
23. Martin, J. H., Knauer, G. A., Karl, D. M. & Broenkow, W. W. Vertex—carbon cycling in the northeast pacific. *Deep-Sea Res.* **34,** 267–285 (1987).
24. Bianchi, D., Dunne, J. P., Sarmiento, J. L. & Galbraith, E. D. Data-based estimates of suboxia, denitrification, and N_2O production in the ocean and their sensitivities to dissolved O_2. *Glob. Biogeochem. Cycles* **26** http://dx.doi.org/10.1029/2011GB004209 (2012).
25. Childress, J. J. & Seibel, B. A. Life at stable low oxygen levels: Adaptations of animals to oceanic oxygen minimum layers. *J. Exp. Biol.* **201,** 1223–1232 (1998).
26. Wyrtki, K. The oxygen minima in relation to ocean circulation. *Deep-Sea Res.* **9,** 11–23 (1962).
27. Keeling, R. F., Kortzinger, A. & Gruber, N. Ocean deoxygenation in a warming world. *Annu. Rev. Mar. Sci.* **2,** 199–229 (2010).
28. Steinberg, D. K., Lomas, M. W. & Cope, J. S. Long-term increase in mesozooplankton biomass in the Sargasso Sea: Linkage to climate and implications for food web dynamics and biogeochemical cycling. *Glob. Biogeochem. Cycles* **26** http://dx.doi.org/10.1029/2010GB004026 (2012).
29. Flagg, C. N. & Smith, S. L. On the use of the acoustic doppler current profiler to measure zooplankton abundance. *Deep-Sea Res. I* **36,** 455–474 (1989).
30. Heywood, K. J., Scropehowe, S. & Barton, E. D. Estimation of zooplankton abundance from ship-borne adcp backscatter. *Deep-Sea Res. I* **38,** 677–691 (1991).

Acknowledgements

The authors thank J. L. Sarmiento and J. P. Dunne for insightful comments on the project, P. Caldwell for kindly providing the JASADCP data and D. Balachandran for preliminary analysis. D.B. and E.D.G. were financially supported by the Canadian Institute for Advanced Research (CIFAR) Earth System Evolution Program. K.A.S. was financially supported by the Carbon Mitigation Initiative with support from BP and the NOAA Cooperative Institute for Climate Science. D.A.C. acknowledges the support of SSHRC of Canada. Computation resources were provided by the SciNet HPC consortium, the Canada Foundation for Innovation and Compute Canada.

Author contributions

D.B. led the data and model analysis and wrote the paper. D.B., E.D.G, K.A.S., D.A.C. and C.A.S. contributed to the interpretation of the data and model results. D.B., E.D.G and D.A.C designed and performed the numerical simulations.

Additional information

Supplementary information is available in the online version of the paper. Reprints and permissions information is available online at www.nature.com/reprints. Correspondence and requests for materials should be addressed to D.B.

Competing financial interests

The authors declare no competing financial interests.

© 2013 Macmillan Publishers Limited. All rights reserved.

nature geoscience

SUPPLEMENTARY INFORMATION

DOI: 10.1038/NGEO1837

Intensification of open-ocean oxygen depletion by vertically migrating animals

Daniele Bianchi, Eric D. Galbraith, David A. Carozza, K.A.S. Mislan, Charles A. Stock

This pdf file includes:

Analysis of the ADCP and estimate of daytime DVM depths

We analyzed 1455 cruises from the US National Oceanic Data Center Joint Archive for Shipboard Acoustic Doppler Current Profilers (ADCPs) and from the British Oceanographic Data Center. We selected 389 cruises that showed at least one detectable DVM event in the ADCP echo intensity signal. Several cruises had to be excluded because they did not allow for the detection of DVM events, owing to a combination of reasons, including ADCP data (1) extending only few hundred meters deep, thus missing the lower parts of DVM events; (2) having too many temporal gaps; (3) being too noisy; (4) having a large proportion of "bad" flags.

To focus on DVM patterns that penetrated into the mesopelagic zone, we excluded migrations shallower than approximately 150-200 m. We excluded all data that were flagged as 'bad', and corrected echo intensities by subtracting the mean of the lowest 10% of the data from each profile to remove background noise.

© 2013 Macmillan Publishers Limited. All rights reserved.

For each detectable DVM event (4640 in total) we estimated the daytime DVM depth from: (1) the maximum subsurface day-to-night echo intensity difference, and (2) the maximum subsurface daytime backscatter. In the first case we calculated the difference in ADCP echo intensity averaged over a 3-hour interval centered at the time of maximum solar elevation (midday) and the ADCP echo intensity averaged over a 3-hour interval centered at the time of minimum solar elevation (midnight) for the nights surrounding the DVM event. We then detected the depth of the maximum subsurface echo intensity difference. In the second case, we estimated the depth of the midday subsurface backscatter maximum. Backscatter was estimated from the ADCP echo intensity by correcting for both sound-wave spherical attenuation and water absorption using the formulation of ref. [1]. The use of the two methods increased the number of records for which the daytime DVM depth could be isolated. Whenever both methods provided a valid daytime DVM depth, the average of the two values was taken.

Overall, the two methods produced similar results (Fig. S1). The estimated daytime DVM depths are the same (within a 8 m bin depth resolution) for 38 % of the events, and differ by less than 50 m for 80 % of the events. Only 7 % of the events showed depths differing by more than 100 m. Some acoustic profiles are characterized by multiple scattering layers with daytime DVM depths generally less than 100 m apart. In the cases where multiple migrating sound scattering layers were present, we isolated the layer that returned the strongest backscatter signal.

The gridded dataset shown in Fig. 2 was generated by averaging the daytime DVM depths in 4° by 4° areas. Fig. S2 and S3 show the number of measurements and standard deviations of the gridded data in each box.

Relationship between light and daytime DVM depths

© 2013 Macmillan Publishers Limited. All rights reserved.

We estimate the ability of water column light intensity to predict daytime DVM depths by calculating the peak irradiance in the water column from observed surface shortwave radiation, climatological profiles of chlorophyll [2], and chlorophyll-dependent light absorption [3,4].

We calculated the light levels and isolume depths at the time and locations of the DVM records by combining daytime surface shortwave radiation from the NOAA Climate Forecast System Reanalysis and chlorophyll-dependent light attenuation coefficients. Chlorophyll profiles were determined using the parameterization of ref.[2] forced with climatological surface chlorophyll from NASA Goddard Center SeaWiFS data, and climatological mixed layer depths[5]. We used the light attenuation scheme of ref. [3] for the full shortwave spectrum, and the light attenuation scheme of ref. [4] for selected shortwave bands in the 400-500 nm range, corresponding to the deepest light penetration in the ocean, and the maximum zooplankton and micronekton vision sensitivities[6].

According to the isolume hypothesis[7], DVM daytime depth should correspond to a small range of light intensities. However, the maximum light intensity over the visible spectrum at the daytime DVM depths varies between 10^{-7} and 10^{-2} W m^{-2} (mean Log_{10} of the irradiance in W m^{-2} of -4.0 ± 0.8, Fig. S4). This wide range of light intensities at the daytime DVM depths (Fig. S4) does not support the existence of a single global isolume determining the depth of migrations. However, it is possible that that light cues are modulated, worldwide, by additional environmental factors, or that distinct populations of migrating organisms respond differently to light stimuli, so that distinct isolumes control migrations in different oceanographic provinces.

At the global scale, the depth of the mean global isolume (10^{-4} W m^{-2}) shows a poor ability in predicting the daytime DVM depths ($R^2 = 0.20$, $p < 0.01$, Fig. S5). Although some of

© 2013 Macmillan Publishers Limited. All rights reserved.

the features of the daytime DVM depths are mirrored by global isolume depths, for example deepening towards the central subtropical gyres, and shallowing towards polar and upwelling regions, isolume depths underestimate the magnitude of DVM depth excursions between such regions. Vertical migrations tend to be deeper than the mean global isolume in the subtropical gyres and in the high latitude South Pacific, and shallower in the Indian Ocean, Eastern Tropical Pacific, and Subarctic Pacific. Similar results hold for wavelength-dependent global isolumes.

Regression between oceanographic property and DVM depth

We tested the ability of different oceanographic variables in predicting daytime DVM depths. Of all the variables considered, the largest significant correlations to daytime DVM depths were found for oxygen, chlorophyll and mixed layer depths. Shallower migrations where observed in regions characterized by lower subsurface oxygen, higher surface chlorophyll and shallower mixed layer depths. A stepwise multiple linear regression also included temperature as a significant predictor. We chose to use the differences between surface and mid-depth oxygen and temperature as predictors in order to represent the range of conditions that migrators experience throughout each DVM cycle. We obtained analogous results, with slightly smaller correlation coefficients, when we used the absolute values of oxygen and temperature instead of surface to mid-depth differences. We used climatological data to calculate the oxygen and temperature differences between 0 - 25 m and 150 - 500 m depth (ΔO_2, mmol m^{-3}, and ΔT, °C), the Log_{10} of surface chlorophyll (Chl, mg m^{-3}) and mixed layer depths (mld, m) at the months and locations of the DVM records. We used monthly climatological oxygen and temperature from the NODC World Ocean Atlas Dataset 2005; monthly climatological chlorophyll from

© 2013 Macmillan Publishers Limited. All rights reserved.

NASA Goddard Center SeaWiFS data, and monthly climatological mixed layer depths from ref. [5]. The resulting daytime DVM depth (m) from a stepwise multiple linear regression is:

$$Z_{DVM} = 398 - 0.56 \cdot \Delta O_2 - 115 \cdot Log_{10}(Chl) + 0.36 \cdot mld - 2.4 \cdot \Delta T$$

with the following 95 % confidence intervals for each term respectively: 391, 405; -0.59, -0.53; -121, -108; 0.31, 0.42; -2.7, -2.1. The root mean square error of the regression is 53 m.

Although more complex models can be designed, a linear regression showed to be sufficient to explain a large proportion of the DVM patterns ($R^2 = 0.60$, $p < 0.01$, Fig. S6). Similar results can be obtained using net primary production (NPP) or export production instead of chlorophyll. However, we chose to use chlorophyll alone because large-scale observational datasets of NPP and export production are based on empirical relationships that use satellite chlorophyll and temperature observations (e.g. Dunne et al., 2007 and references therein), and thus do not represent truly independent variables. Physical and biogeochemical properties vary in concert in the ocean and are not completely uncorrelated. However, within the uncertainty bounds, we obtained the same regression coefficients after linear regularization of the regression.

Diel vertical migrations and oxygen profiles

The global analysis in Fig. 1, and the results from the multiple linear regression analysis show shallow migrations in the major open ocean OMZs, to depths that correspond to hypoxic and suboxic concentrations, and deeper migrations in well oxygenated waters. Inspection of DVM depths in relation to oxygen profiles (Fig. S7) indicates that in regions where oxygen minima are present, migrators reach well within the hypoxic (O_2<60 mmol m^{-3}) and, where present, suboxic (O2<5 mmol m^{-3}) domains, often spending the daytime in proximity of the core of the OMZ, as

© 2013 Macmillan Publishers Limited. All rights reserved.

in the case of the shallower South Eastern Tropical Pacific, North Eastern Tropical Atlantic, South Eastern Tropical Atlantic, and Bay of Bengal oxygen minima. This association between DVM and oxygen minima supports and extend previous local surveys[8-10], and is consistent with the hypothesis that hypoxic and suboxic waters might provide a refuge from large predators with high oxygen requirements[11,12].

Ocean Circulation-Biogeochemistry Model

The model used in this study is the 3-degree resolution GFDL MOM4p1 ocean model coupled with the BLINGv0 biogeochemistry model[13]. MOM4p1 is a pressure coordinate, free-surface ocean model that includes parameterizations of mesoscale and sub-submesoscale processes and mixed layer dynamics. The model is forced with heat, freshwater and shortwave fluxes from climatologies. BLING is a computationally efficient biogeochemical model consisting of four explicit tracers (dissolved inorganic and organic phosphorous, iron and oxygen) with a representation of macronutrient, micronutrient, and light limitation, and an implicit treatment of ecosystem community structure. Organic matter production by photosynthesis is partitioned between an explicit dissolved pool and implicit sinking particle and DVM fluxes.

We assume that DVM fluxes are a constant fraction of the organic matter export production, and we vary this fraction between 0 and 0.45, spanning the range of existing observational and model estimates listed in the Supplementary Table S1.

Particle respiration that is not associated with DVM follows a typical observationally-based power law profile[14]. DVM active transport is returned to the water column via a migratory respiration flux, assumed to be uniform between the surface and the daytime DVM depth, and a deep respiration flux shaped as a Gaussian, centered at the daytime DVM depth, with a scale

© 2013 Macmillan Publishers Limited. All rights reserved.

parameter of 50 m, in agreement with observations[9,15] and previous modeling studies[16]. The partitioning between migratory and deep respiration fractions is scaled according to the duration of migrations, assumed to be proportional to the local DVM depth. The DVM depth is determined in the model using the multiple linear regression equation and is shown in Fig. S8. This redistribution presumes that the respiration associated with organic material consumed near the surface continues throughout the day. To simulate the lack of diurnal migrations in the wintertime high latitudes, the DVM depth is linearly decreased to 150 m when the daily mean surface irradiance decreases below 10 W m^{-2}. Oxygen consumption by respiration is calculated from the phosphate remineralization rate using a stoichiometric ratio of 150:1, and is set to zero at oxygen concentrations below 1.0 mmol m^{-3}. The profiles of respiration due to the active DVM transport and to the remineralization of passive detritus are shown in Fig. S9 for DVM export fractions equal to 0.15, 0.30 and 0.45. The models were integrated for 1500 years until approximate equilibrium was reached, and the last 100 years of simulations were analyzed.

In the models, the oxygen utilization due to migrators shows an approximately linear dependency with the active export fraction at any given location (Fig. S10). That means that, for example, a doubling of the active export fraction results in a doubling of the oxygen consumption due to vertically migrating organisms. This result allows us to use the different model runs to calculate the slope between the active export fraction and the oxygen utilization due to DVM and express it in units of mmol m^{-3} per each % of export by DVM relative to particle export, as shown in Fig 3. We note that a mechanistic model of migrator biomass, together with specific respiration rates, could be used to quantify the impact of animal respiration on oxygen instead of adopting a fixed DVM export fraction. This would require a predictive model of zooplankton and micronekton

© 2013 Macmillan Publishers Limited. All rights reserved.

biomass, and of the proportion of migrators. While global models have only recently started to simulate animal biomass adequately, a predictive framework for the fraction of migrators is still lacking. The theoretical and observational uncertainties surrounding the migrating fraction and the DVM export persuaded us to express the oxygen utilization due to DVM as a function of the active export fraction (Fig. 3). Together with the range of active export fractions reviewed in Table S1, this can be directly used to estimate the effects of migrations on water column chemistry and oxygen distribution in a general sense.

© 2013 Macmillan Publishers Limited. All rights reserved.

Supplementary Table S1. Observational and model-based estimates of active organic matter export relative to particle export (DVM/POC export, percent).

Location	DVM/POC export (%)	Reference
Median of 9 oceanic sites(1)	26	17
North Atlantic (NFLUX) (2)	8	18
Eastern Tropical Pacific (2 sites) (3)	25-45	19
Subtropical North Atlantic and North Atlantic (5 sites) (3)	14-53	19
Subtropical North Atlantic (BATS) (4)	34 (18-70)	20
Equatorial Pacific (EqPac) (5)	31-44	21
North Atlantic (NABE) (6)	19-40	22
Subtropical North Atlantic (BATS) (7)	8 (0-39)	23
Subtropical North Pacific (ALOHA) (8)	15	24
Western Equatorial Pacific (9)	30-48 (uncorrected) 50-100 (corrected)	25
Subtropical North Atlantic (Canary Islands) (10)	25 (16-45)	26
Subtropical North Atlantic (Canary Islands) (11)	15-53	27
Subtropical North Pacific (12)	20	28
Subtropical North Atlantic (BATS) (13)	15	29
North Pacific Ocean (subpolar to equatorial) (14)	15-40	16

(1) Longhurst and Harrison (1988) (ref. [17]). Biomass data for migratory zooplankton and micronekton from 9 stratified low-latitude sites are used in conjunction with estimates of excretion rates to calculate the DVM active transport. Primary production data are used to estimate the particle flux at 100 m depth.

© 2013 Macmillan Publishers Limited. All rights reserved.

(2) Longhurst et al. (1989) (ref. [18]). NFLUX station (38N, 65W). Export fluxes out of the euphotic zone (100-120 m). DVM active transport estimated from $NH4^+$ excretion rates; particle flux from sediment trap data.

(3) Longhurst et al. (1990) (ref. [19]). Export fluxes across the upper ocean density discontinuity (47-100 m in the Eastern Tropical Pacific; 58-200 m in the Subtropical Atlantic). DVM active transport estimated from migratory mesozooplankton and micronekton biomass together with estimates of excretion rates from the literature; particle flux is calculated from primary production measurements.

(4) Dam et al. (1995) (ref. [20]). JGOFS BATS station (31N, 64W). DVM export fluxes at 150 m depth from daytime and nighttime mesozooplankton biomass measurements combined with published metabolic rates. Particle fluxes at 150 m depth from sediment traps.

(5) Zhang and Dam (1997) (ref. [21]). JGOFS EqPac station (0N,140W). DVM export fluxes from the euphotic zone estimated from daytime and nighttime mesozooplankton biomass measurements combined with published metabolic rates. Particle fluxes from the euphotic zone from sediment traps.

(6) Morales (1999) (ref. [22]). JGOFS NABE cruises (3 cruises between 41N-63N and 14W-18W). DVM (mesozooplankton) and particle export fluxes out of the surface layers (100 m depth) from literature and JGOFS-NABE data in the North Atlantic.

(7) Steinberg et al. (2000) (ref. [23]). JGOFS BATS site (31N, 64W). DVM export fluxes at 150 m depth from daytime and nighttime mesozooplankton biomass measurements combined with metabolic rate estimates from the literature. Particle fluxes at 150 m depth from sediment traps.

(8) Al-Mutahiri and Landry (2001) (ref. [24]). Station ALOHA (22N, 158W). DVM export fluxes at 155 m depth from daytime and nighttime mesozooplankton biomass measurements combined with metabolic rate estimates from the literature. Particle fluxes at 150 m depth from sediment traps.

(9) Hidaka et al. (2001) (ref. [25]). Western equatorial Pacific (3N-145W). DVM export fluxes at 160 m depth from daytime and nighttime mesozooplankton and micronekton biomass measurements combined with metabolic rate estimates from the literature. Particle fluxes at 160 m depth from sediment traps. The corrected values include an upward estimate of the migratory micronekton biomass obtained by assuming a 14 % micronekton sampling effciency of the trawls.

(10) Hernandez Leon et al. (2001) (ref. [26]). Canary Islands. DVM export fluxes at 200 m depth from daytime and nighttime mesozooplankton biomass measurements combined with in situ metabolic rate measurements. Particle fluxes at 150 m depth from literature data.

(11) Yebra et al. (2005) (ref. [27]). For methods, see (10).

(12) Hannides et al. (2009) (ref. [28]). Station ALOHA (22N, 158W). DVM export fluxes at 160 m depth from daytime and nighttime mesozooplankton biomass measurements combined with metabolic rate estimates from the literature. Particle fluxes at 150 m depth from sediment traps.

© 2013 **Macmillan Publishers Limited. All rights reserved.**

(13)Steinberg et al., (2012) (ref. [29]). 17-year timeseries at the JGOFS BATS site (31N, 64W). DVM export fluxes at 150 m depth from daytime and nighttime mesozooplankton biomass measurements combined with metabolic rate estimates from the literature. Particle fluxes at 150 m depth from sediment traps.

(14) Bianchi et al. (in press) (ref.[16]). Modelling study based on a 1-D multiple size-class NPZD model which includes explicit representation of DVM dynamics, calibrated against observed productivity and biomasses for three sites in the Pacific Ocean.

© 2013 **Macmillan Publishers Limited. All rights reserved.**

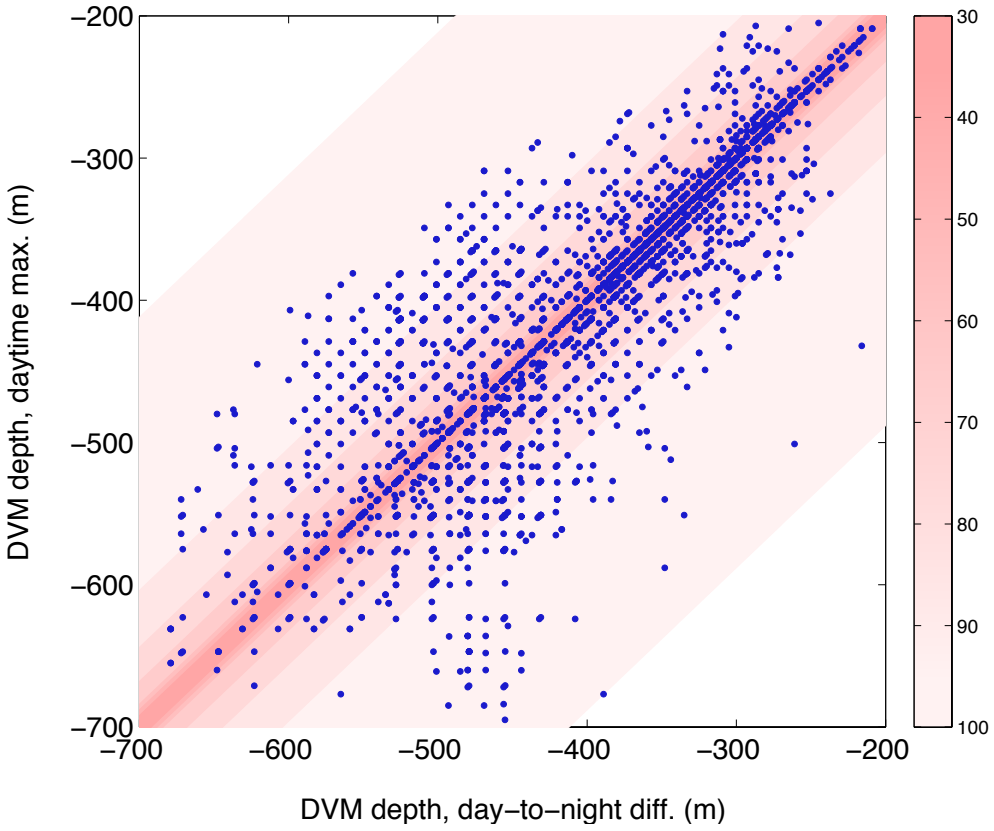

Figure S1. Relationship between different estimates of DVM depth. The figure shows a scatter plot of the DVM depth from daytime maximum subsurface backscatter versus DVM depth from day-to-night ADCP amplitude difference. The colour shading shows the density distribution of the data (percent). 30 % of the data show identical depths; 80 % of the data show differences less than 50 m.

© 2013 Macmillan Publishers Limited. All rights reserved.

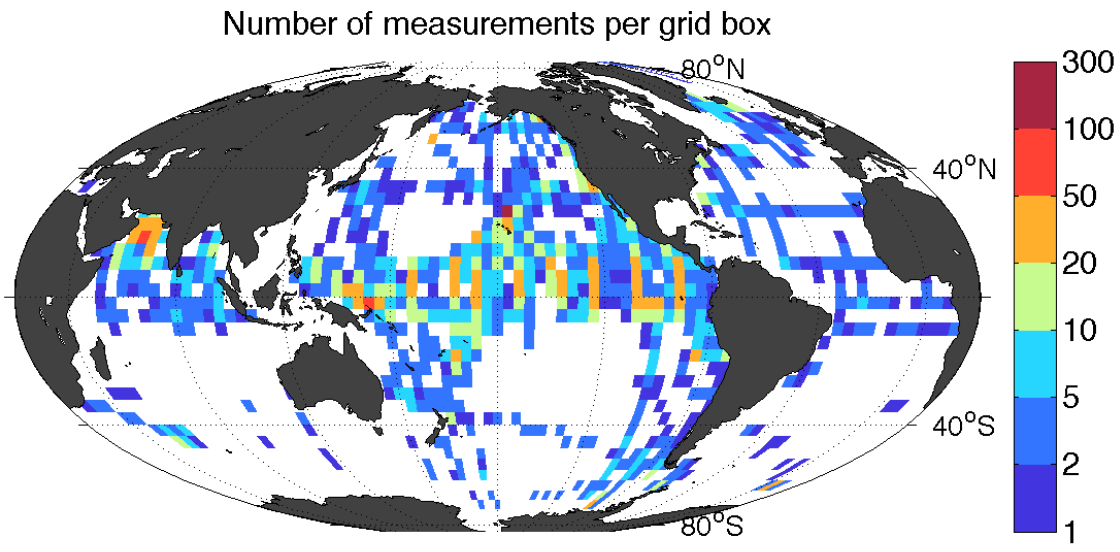

Figure S2. **Number of DVM depth observations.** The figure shows the number of DVM events detected in the ADCP data for each of the 4° by 4° areas used to generate Fig. 2.

© 2013 Macmillan Publishers Limited. All rights reserved.

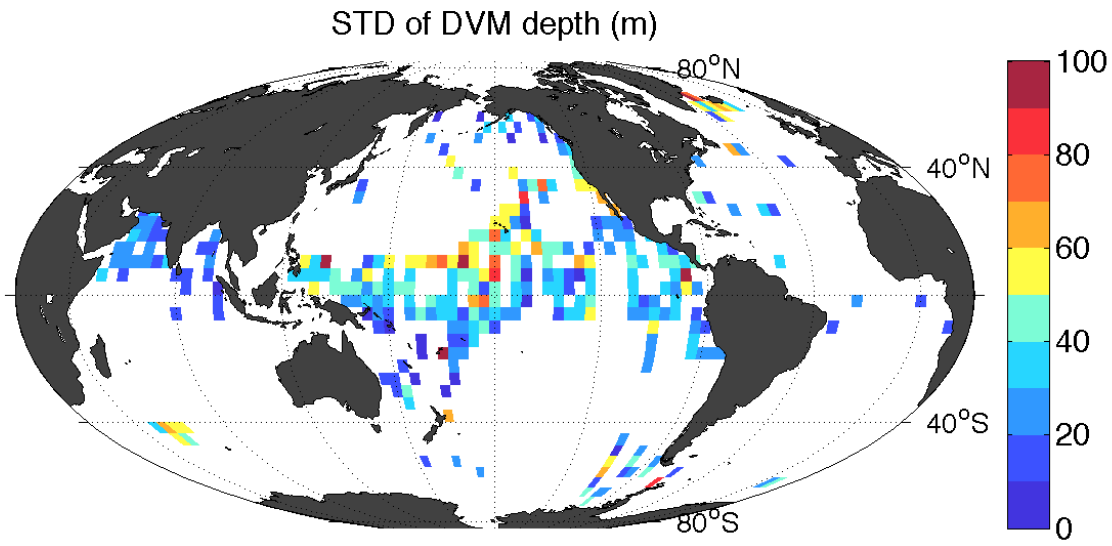

Figure S3. **Standard deviations of DVM depths.** The figure shows the standard deviation of the DVM depths for each of the 4° by 4° areas shown in Fig. 2. Values are shown only for grid areas containing 3 DVM depth estimates or more.

© 2013 Macmillan Publishers Limited. All rights reserved.

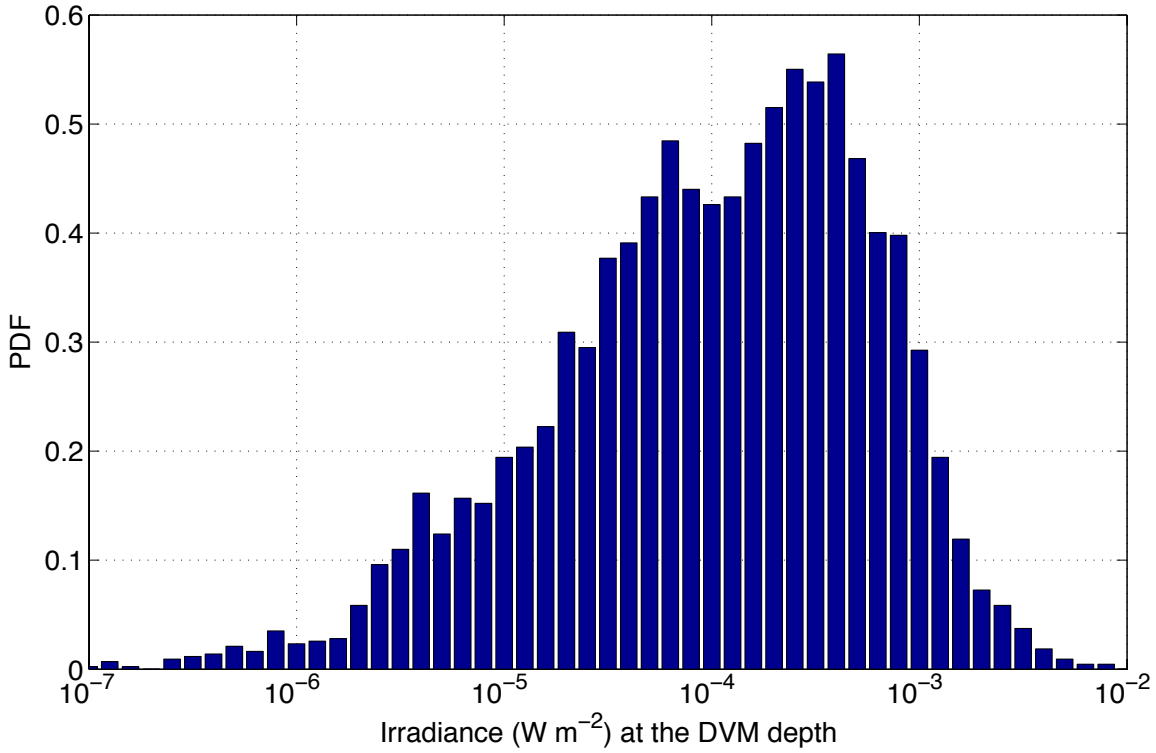

Figure S4. **Probability distribution function of the irradiance (W m^{-2}) at the daytime DVM depth.** The probability distribution was calculated by dividing the number of measurements in each irradiance bin by the bin width. The irradiance was estimated using the light penetration scheme of ref. [3] using surface irradiance and depth-dependent chlorophyll from climatologies.

© 2013 Macmillan Publishers Limited. All rights reserved.

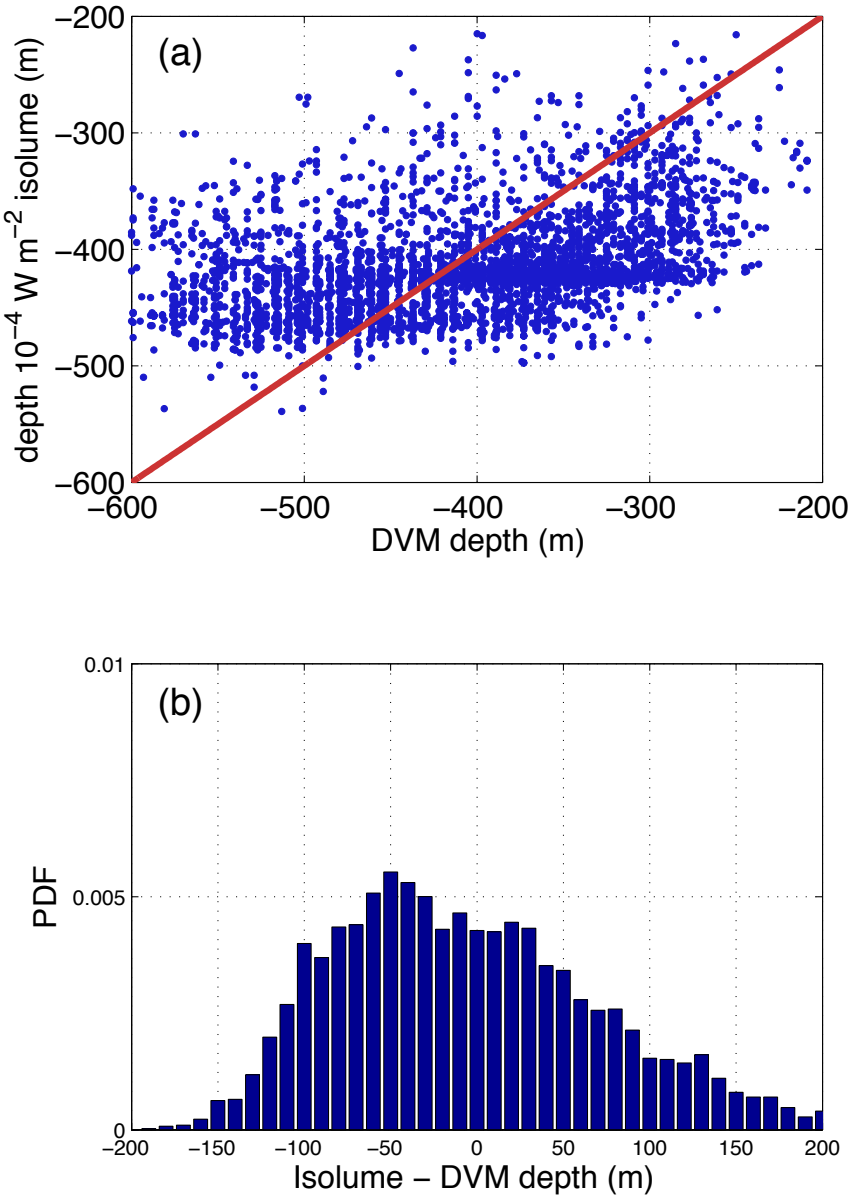

Figure S5. Daytime DVM depth predicted from global isolume depth. (**A**) Scatter plot of the depth of the mean isolume (10^{-4} Wm^{-2}) versus the DVM depth. The correlation coefficient is $R^2 = 0.20$ ($p < 0.01$). The red line is the 1:1 line. (**B**) Probability distribution function of the difference between isolume depth and daytime DVM depth. The probability distribution was calculated by dividing the number of measurements in each depth bin by the bin width. The mean and standard deviation of the distribution are 0 and 80 m respectively.

© 2013 Macmillan Publishers Limited. All rights reserved.

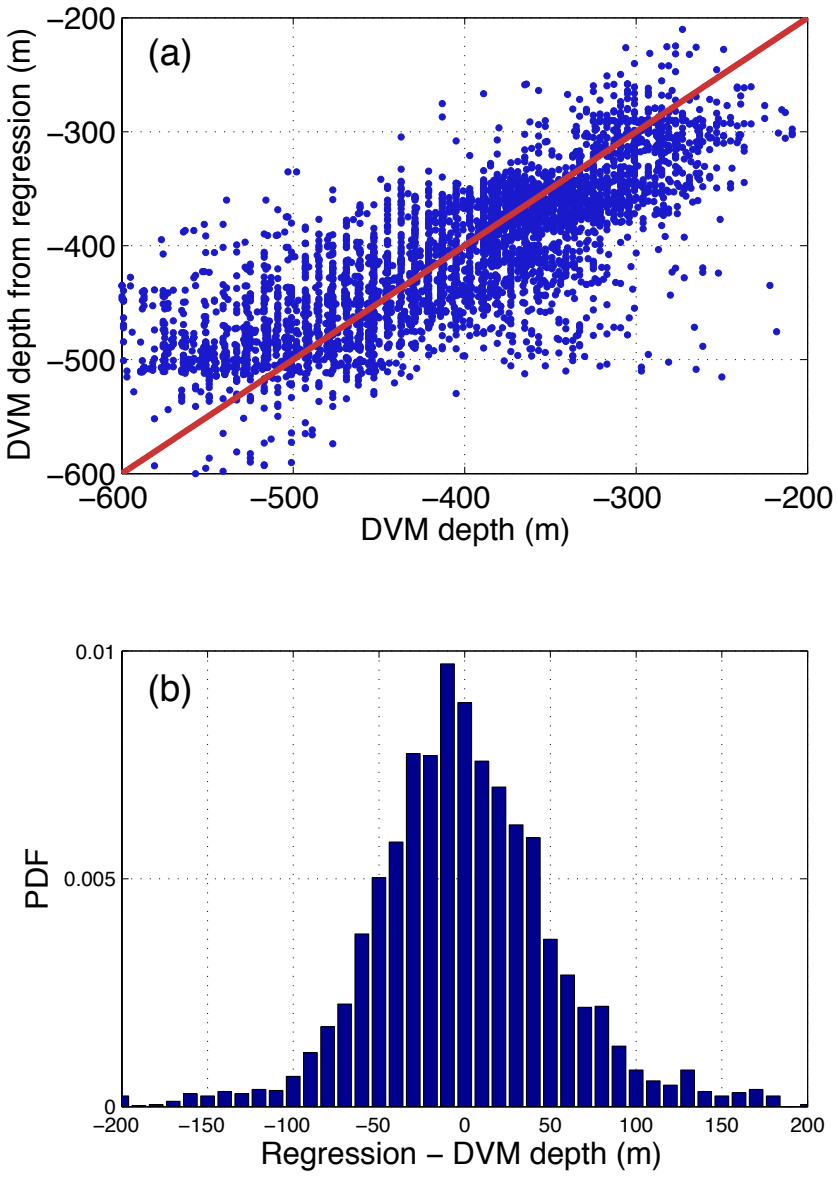

Figure S6. Daytime DVM depth predicted from environmental variables. (**A**) Scatter plot of the DVM depth estimated from a stepwise multiple linear regression versus the actual DVM depth. The coefficient of determination of the regression is $R^2 = 0.60$ ($p < 0.01$). The red line is the 1:1 line. (**B**) Probability distribution function of the difference between daytime DVM depth from the regression and observed daytime DVM depth. The probability distribution was calculated by dividing the number of measurements in each depth bin by the bin width. The mean and standard deviation of the distribution are 0 and 54 m respectively.

© 2013 Macmillan Publishers Limited. All rights reserved.

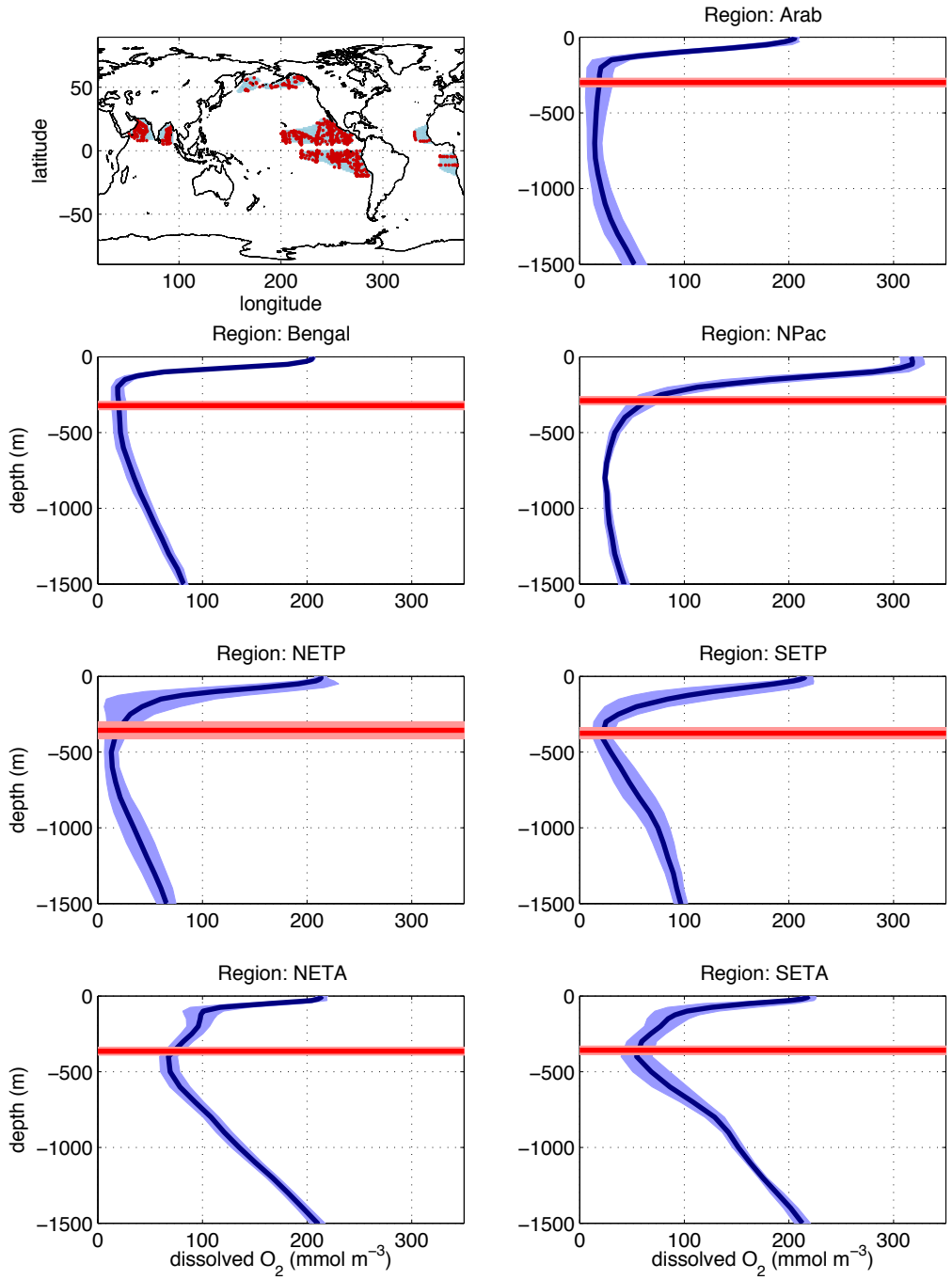

Figure S7. **Relationship between daytime DVM depths and oxygen profiles.** The first panel shows a map of the 7 major open ocean oxygen minimum zones (blue shading) and the locations of single DVM events detected in the acoustic data within each of the regions (red dots.) The following panels show in blue the average oxygen profiles (mmol m^{-3}) from each region from the

© 2013 Macmillan Publishers Limited. All rights reserved.

World Ocean Atlas, and in red the location of the average DVM depth detected in the acoustic data. Shadings show one standard deviation around the means. The regions are: Arabian Sea, Bay of Bengal, North Pacific, North Eastern Tropical Pacific, South Eastern Tropical Pacific, North Eastern Tropical Atlantic, South Eastern Tropical Atlantic.

© 2013 Macmillan Publishers Limited. All rights reserved.

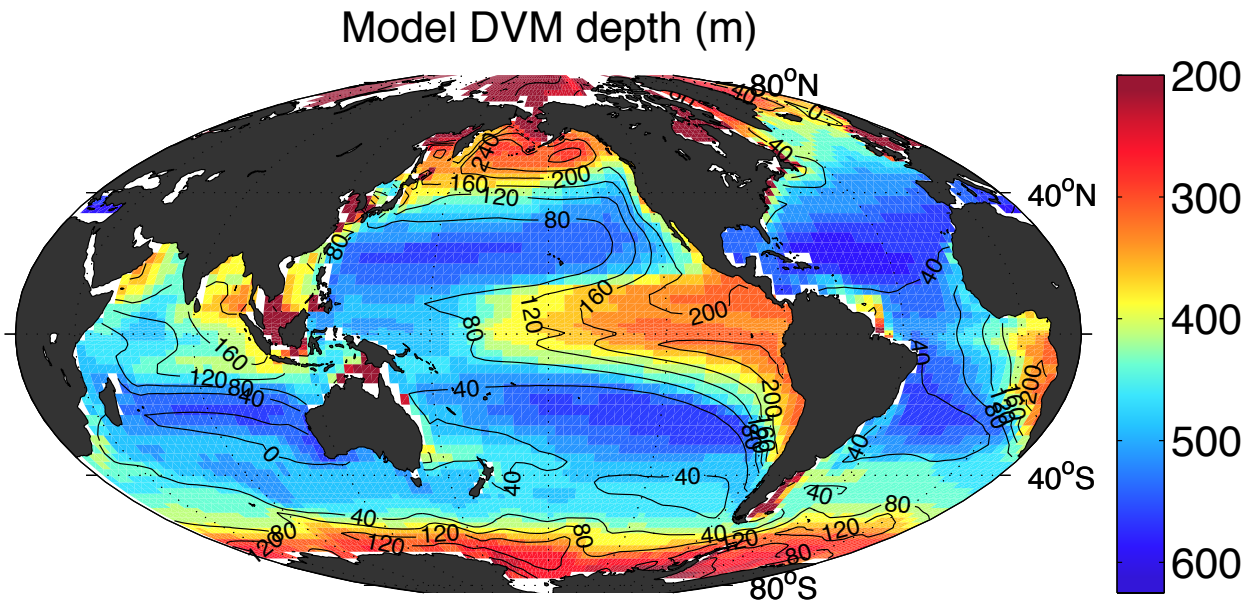

Figure S8. **Annual mean DVM depth (m) in the model.** Daytime DVM depths (colours) predicted using the regression of equation S1, using model temperature, oxygen, chlorophyll and mixed layer depths. Contours show the surface (0 - 25 m) to upper mesopelagic zone (150 - 500 m) oxygen difference (mmol m^{-3}).

© 2013 Macmillan Publishers Limited. All rights reserved.

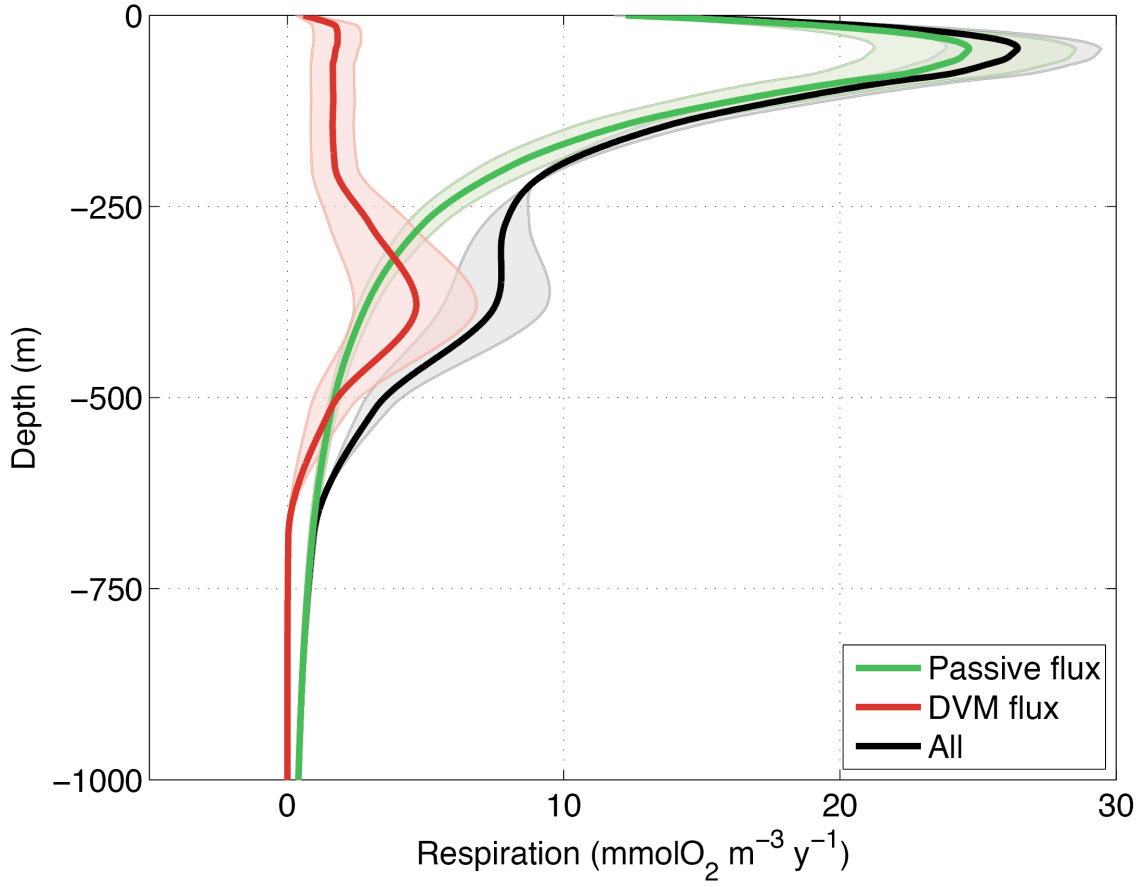

Figure S9. **Globally averaged respiration (mmol m^{-3} $year^{-1}$) in the model**. The green line shows the passive detritus respiration (sinking particles and dissolved organic matter), the red line shows the respiration due to active DVM transport, and the black line the sum of the two. Results are shown for active DVM flux equal to 0.3 times the organic matter export production. The light-coloured shadings indicate the envelope values obtained with active DVM fractions equal to 0.15 and 0.45 times the organic matter export production respectively.

© 2013 Macmillan Publishers Limited. All rights reserved.

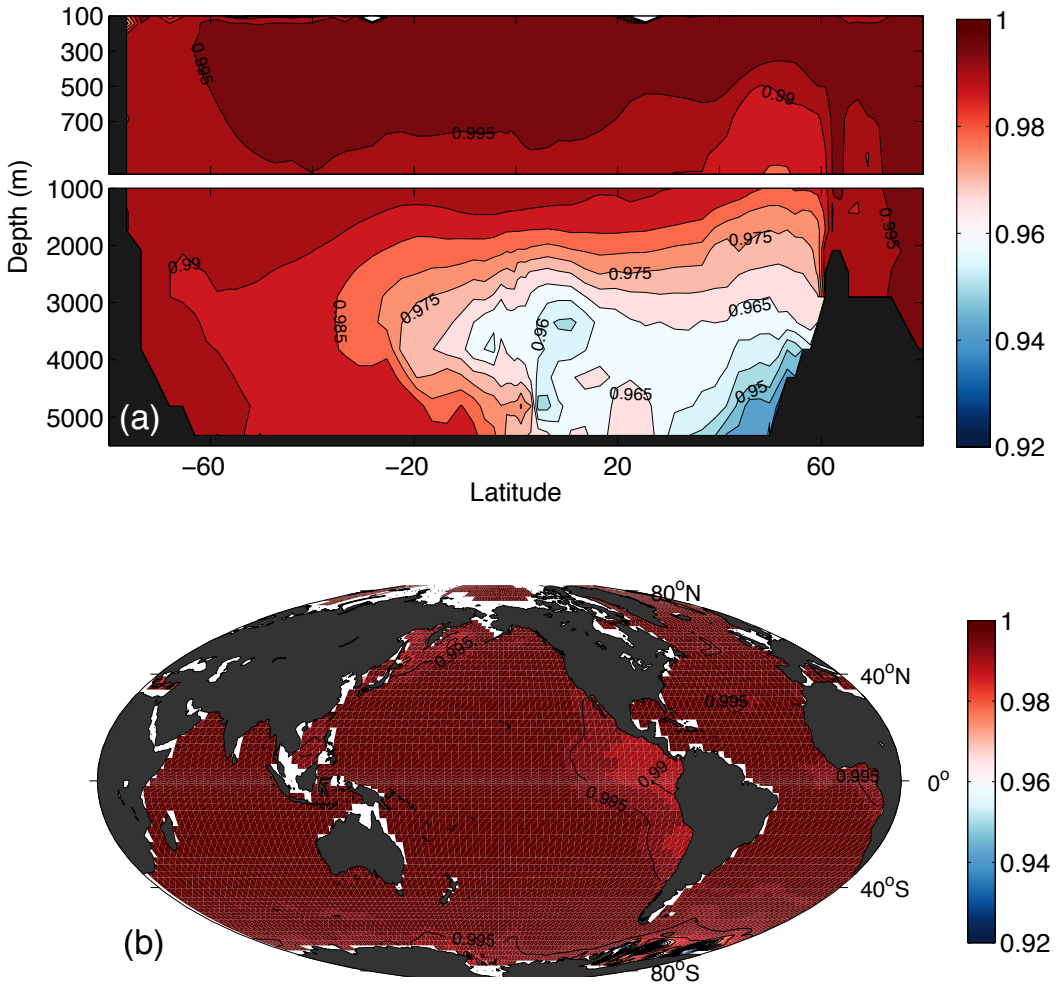

Figure S10. **Correlation between the active export fraction and the oxygen utilization due to DVM in the model**. The correlation coefficients were calculated at each model grid point, using the oxygen utilization due to DVM from 4 model runs where the active export fraction was varied between 0 and 0.45. (A) Zonal average. Values shallower than 100 m were excluded because approaching the surface oxygen utilizations tend to zero resulting in noisy correlations. Lower correlation in the abyssal ocean might be due to incomplete model equilibration after the 1500 year spin up. (B) Average over the upper mesopelagic zone (150 - 500 m).

© 2013 Macmillan Publishers Limited. All rights reserved.

Supplementary References

1 Deines, K. L. Backscatter estimation using broadband acoustic Doppler Current Profilers. *Proceedings of the Ieee Sixth Working Conference on Current Measurement*, 249-253 (1999).

2 Uitz, J., Claustre, H., Morel, A. & Hooker, S. B. Vertical distribution of phytoplankton communities in open ocean: An assessment based on surface chlorophyll. *J Geophys Res-Oceans* **111** (2006).

3 Manizza, M., Le Quere, C., Watson, A. J. & Buitenhuis, E. T. Bio-optical feedbacks among phytoplankton, upper ocean physics and sea-ice in a global model. *Geophys Res Lett* **32** (2005).

4 Morel, A. & Maritorena, S. Bio-optical properties of oceanic waters: A reappraisal. *J Geophys Res-Oceans* **106**, 7163-7180 (2001).

5 Montegut, C. D., Madec, G., Fischer, A. S., Lazar, A. & Iudicone, D. Mixed layer depth over the global ocean: An examination of profile data and a profile-based climatology. *J Geophys Res-Oceans* **109** (2004).

6 Warrant, E. J. & Locket, N. A. Vision in the deep sea. *Biol Rev* **79**, 671-712 (2004).

7 Cohen, J. H. & Forward, R. B. Zooplankton Diel Vertical Migration - a Review of Proximate Control. *Oceanogr Mar Biol* **47**, 77-109 (2009).

8 Barham, E. G. Deep Scattering Layer Migration and Composition - Observations from a Diving Saucer. *Science* **151**, 1399-& (1966).

9 Luo, J. G., Ortner, P. B., Forcucci, D. & Cummings, S. R. Diel vertical migration of zooplankton and mesopelagic fish in the Arabian Sea. *Deep-Sea Res Pt Ii* **47**, 1451-1473 (2000).

10 Ashjian, C. J., Smith, S. L., Flagg, C. N. & Idrisi, N. Distribution, annual cycle, and vertical migration of acoustically derived biomass in the Arabian Sea during 1994-1995. *Deep-Sea Res Pt Ii* **49**, 2377-2402 (2002).

11 Seibel, B. A. Critical oxygen levels and metabolic suppression in oceanic oxygen minimum zones. *J Exp Biol* **214**, 326-336 (2011).

12 Stramma, L. *et al.* Expansion of oxygen minimum zones may reduce available habitat for tropical pelagic fishes. *Nat Clim Change* **2**, 33-37 (2012).

13 Galbraith, E. D., Gnanadesikan, A., Dunne, J. P. & Hiscock, M. R. Regional impacts of iron-light colimitation in a global biogeochemical model. *Biogeosciences* **7**, 1043-1064 (2010).

14 Martin, J. H., Knauer, G. A., Karl, D. M. & Broenkow, W. W. Vertex - Carbon Cycling in the Northeast Pacific. *Deep-Sea Research Part a-Oceanographic Research Papers* **34**, 267-285 (1987).

15 Steinberg, D. K., Cope, J. S., Wilson, S. E. & Kobari, T. A comparison of mesopelagic mesozooplankton community structure in the subtropical and subarctic North Pacific Ocean. *Deep-Sea Res Pt Ii* **55** (2008).

16 Bianchi, D., Stock, C., Galbraith, E. D. & Sarmiento, J. L. Diel vertical migration: ecological controls and impacts on the biological pump in a one-dimensional ocean model. *Global Biogeochemical Cycles, in press* (2013).

© 2013 **Macmillan Publishers Limited. All rights reserved.**

17 Longhurst, A. R. & Harrison, W. G. Vertical Nitrogen Flux from the Oceanic Photic Zone by Diel Migrant Zooplankton and Nekton. *Deep-Sea Research Part a-Oceanographic Research Papers* **35**, 881-889 (1988).
18 Longhurst, A. R. *et al.* Nflux - a Test of Vertical Nitrogen Flux by Diel Migrant Biota. *Deep-Sea Res* **36**, 1705-1719 (1989).
19 Longhurst, A. R., Bedo, A. W., Harrison, W. G., Head, E. J. H. & Sameoto, D. D. Vertical Flux of Respiratory Carbon by Oceanic Diel Migrant Biota. *Deep-Sea Research Part a-Oceanographic Research Papers* **37**, 685-694 (1990).
20 Dam, H. G., Roman, M. R. & Youngbluth, M. J. Downward Export of Respiratory Carbon and Dissolved Inorganic Nitrogen by Diel-Migrant Mesozooplankton at the Jgofs Bermuda Time-Series Station. *Deep-Sea Res Pt I* **42**, 1187-1197 (1995).
21 Zhang, X. S. & Dam, H. G. Downward export of carbon by diel migrant mesozooplankton in the central equatorial Pacific. *Deep-Sea Res Pt Ii* **44**, 2191-2202 (1997).
22 Morales, C. E. Carbon and nitrogen fluxes in the oceans: the contribution by zooplankton migrants to active transport in the North Atlantic during the Joint Global Ocean Flux Study. *J Plankton Res* **21**, 1799-1808 (1999).
23 Steinberg, D. K. *et al.* Zooplankton vertical migration and the active transport of dissolved organic and inorganic carbon in the Sargasso Sea. *Deep-Sea Res Pt I* **47**, 137-158 (2000).
24 Al-Mutairi, H. & Landry, M. R. Active export of carbon and nitrogen at Station ALOHA by diel migrant zooplankton. *Deep-Sea Res Pt Ii* **48**, 2083-2103 (2001).
25 Hidaka, K., Kawaguchi, K., Murakami, M. & Takahashi, M. Downward transport of organic carbon by diel migratory micronekton in the western equatorial Pacific: its quantitative and qualitative importance. *Deep-Sea Res Pt I* **48**, 1923-1939 (2001).
26 Hernandez-Leon, S. *et al.* Vertical distribution of zooplankton in Canary Island waters: implications for export flux. *Deep-Sea Res* **48**, 1071-1092 (2001).
27 Yebra, L., Almeida, C. & Hernandez-Leon, S. Vertical distribution of zooplankton and active flux across an anticyclonic eddy in the Canary Island waters. *Deep-Sea Res Pt I* **52**, 69-83 (2005).
28 Hannides, C. C. S. *et al.* Export stoichiometry and migrant-mediated flux of phosphorus in the North Pacific Subtropical Gyre. *Deep-Sea Res Pt I* **56**, 73-88 (2009).
29 Steinberg, D. K., Lomas, M. W. & Cope, J. S. Long-term increase in mesozooplankton biomass in the Sargasso Sea: Linkage to climate and implications for food web dynamics and biogeochemical cycling. *Global Biogeochem Cy* **26** (2012).

© 2013 **Macmillan Publishers Limited. All rights reserved.**